AD-A083 391   NAVAL RESEARCH LAB   WASHINGTON DC   F/G 9/5
                NONLINEAR SPECTRAL ANALYSIS AND ADAPTIVE ARRAY SUPERRESOLUTION --ETC(U)
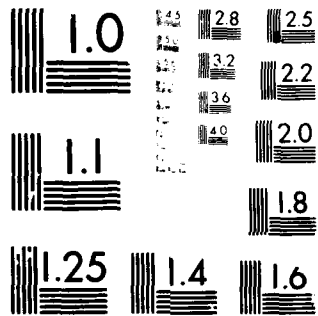   FEB 80   W F GABRIEL
UNCLASSIFIED   NRL-8345   SBIE-AD-E000 390   NL

[OF]
AD
A083391

END
DATE
FILMED

DTIC

MICROCOPY RESOLUTION TEST CHART

NATIONAL BUREAU OF STANDARDS-1963-A

AD-E000 390

(12) **LEVEL** III

Nonlinear Spectral Analysis and Adaptive Array Superresolution Techniques

WILLIAM F. GABRIEL

Antenna Systems Staff
Radar Division

February 1, 1980

DTIC
ELECTE
APR 24 1980

S   D

B

ADA083391

DDC FILE COPY

80   2   28   006

REPORT DOCUMENTATION PAGE		READ INSTRUCTIONS BEFORE COMPLETING FORM
1. REPORT NUMBER NRL Report 8345	2. GOVT ACCESSION NO. AD-A083 391	3. RECIPIENT'S CATALOG NUMBER
4. TITLE (and Subtitle) NONLINEAR SPECTRAL ANALYSIS AND ADAPTIVE ARRAY SUPERRESOLUTION TECHNIQUES		5. TYPE OF REPORT & PERIOD COVERED Interim report on a continuing NRL Problem.
		6. PERFORMING ORG. REPORT NUMBER
7. AUTHOR(s) William F. Gabriel		8. CONTRACT OR GRANT NUMBER(s)
9. PERFORMING ORGANIZATION NAME AND ADDRESS Naval Research Laboratory Washington, DC 20375		10. PROGRAM ELEMENT, PROJECT, TASK AREA & WORK UNIT NUMBERS 61153N, RR021-05-41 R12-46.101 and R08-80.301 NRL Problems WR2101002
11. CONTROLLING OFFICE NAME AND ADDRESS Department of the Navy Department of the Navy Office of Naval Research Naval Air Systems Command Arlington, VA 22217 Washington, D.C. 20361		12. REPORT DATE February 1, 1980
		13. NUMBER OF PAGES 27
14. MONITORING AGENCY NAME & ADDRESS(If different from Controlling Office)		15. SECURITY CLASS. (of this report) UNCLASSIFIED
		15a. DECLASSIFICATION/DOWNGRADING SCHEDULE

16. DISTRIBUTION STATEMENT (of this Report)

Approved for public release; distribution unlimited.

17. DISTRIBUTION STATEMENT (of the abstract entered in Block 20, if different from Report)

18. SUPPLEMENTARY NOTES

19. KEY WORDS (Continue on reverse side if necessary and identify by block number)

Adaptive arrays
Antennas
Nonlinear Processing
Spectral analysis

20. ABSTRACT (Continue on reverse side if necessary and identify by block number)

Two nonlinear spectral analysis techniques, the Burg maximum entropy method and the maximum likelihood method, are related to their similar nonlinear adaptive array antenna counterparts, which consist of the sidelobe canceller and directional gain constraint techniques. The comparison analysis permits an examination of their principles of operation from the antenna spatial pattern viewpoint, and helps to qualify their superresolution performance. The real-time adaptive resolution of two incoherent sources located within a beamwidth was simulated, and results are presented in the form of a universal superresolution curve over a SNR range of 0 to 40 dB. Two alternative adaptive spatial

(Continues)

DD FORM 1473 EDITION OF 1 NOV 65 IS OBSOLETE   i
1 JAN 73
S/N 0102-014-6601

20. Abstract (Continued)

spectrum estimators are suggested, consisting of a circular array predicting to its center point, and a new "thermal noise" algorithm.

CONTENTS

DTIC
SELECTED
APR 2 4 1980
B

ACCESSION for
NTIS	White Section	☑
DDC	Buff Section	☐
UNANNOUNCED		☐
JUSTIFICATION		

BY
DISTRIBUTION/AVAILABILITY CODES
Dist.	AVAIL. and/or SPECIAL
A	

iii

NONLINEAR SPECTRAL ANALYSIS AND ADAPTIVE ARRAY
SUPERRESOLUTION TECHNIQUES

INTRODUCTION

Nonlinear spectral analysis techniques are currently of intense interest because of reported "superresolution" capabilities beyond the conventional periodogram or the Blackman-Tukey windowed Fourier transform [1]. Two methods, in particular, which have demonstrated a considerable increase in resolution are the maximum entropy spectral analysis (MESA) technique introduced by J. P. Burg [2,3], and the maximum likelihood method (MLM) demonstrated by J. Capon [4-6]. Since these techniques are most significant when processing short data sets, it is natural to consider their use for RF array antennas with a modest number of elements [7,8].

Adaptive processing techniques have been associated with these spectral estimation methods to some extent [9-11], but the literature indicates that cross-fertilization has been rather sparse. This situation is surprising, because both MESA and MLM bear a very close relationship to nonlinear adaptive array processing techniques. It is the purpose of this report to relate the MESA and MLM methods to their similar adaptive array antenna counterparts. The comparison analysis permits an examination of their principles of operation from the antenna array spatial pattern viewpoint, and helps to qualify their superresolution performance behavior. The real-time adaptive resolution of two incoherent sources located within a beamwidth has been simulated, and results are presented over an array output signal-to-noise ratio (SNR) range of 0 to 40 dB. The difficulties involved in resolving more than two closely spaced sources are also treated.

In addition to a discussion on the similarities between MESA, MLM, and adaptive array processing, some attention is given to the significant differences, which include the matter of two-dimensional data and the particular manner of averaging or estimating interelement signal correlations.

Alternate techniques for estimating spatial spectra have suggested themselves during the course of this study, and two of these are briefly described in the section on alternate adaptive processing (pp. 19, 20): phase center prediction utilizing a circular array, and a new adaptive "thermal noise" algorithm.

BURG MESA LINEAR PREDICTION FILTER

The Burg MESA method has been shown by van den Bos [12] to be equivalent to least mean square (LMS) error linear prediction. It runs a K-point linear prediction filter across a data sequence of N samples, where N should be at least twice the value of K. In the

discrete filter diagram of Fig. 1, an optimum K-point prediction filter predicts the nth value of the sequence from K past values,

$$\hat{X}_n = \sum_{k=1}^{K} A_k X_{n-k},\tag{1}$$

where $\hat{X}_n$ is the predicted sample, the A_k are optimum weighting coefficients, and the K past samples of X_{n-k} are presumed known. To define the difference between this predicted value and the current true value of X_n as the error ϵ_n, which is to be LMS minimized, we set

$$\epsilon_n = X_n - \hat{X}_n .\tag{2}$$

We minimize the total squared error E over the complete data sequence of N samples,

$$E = \sum_{n=K}^{N-1} \epsilon_n^2\tag{3}$$

and

$$\frac{\partial E}{\partial A_i} = 0, \qquad 1 \leqslant i \leqslant K,\tag{4}$$

thus obtaining a set of K equations in K unknowns, i.e., the A_k filter weights,

$$\sum_{k=1}^{K} A_k \phi_{ki} = -\phi_{0i} \qquad \begin{array}{l} 1 \leqslant k \leqslant K \\ 1 \leqslant i \leqslant K \end{array}\tag{5}$$

$$\phi_{ki} = \sum_{n=k}^{N-1} X_{n-k} X_{n-i}.\tag{6}$$

There are several different techniques, including Burg's, for manipulating this set of equations to solve for the optimum A_k filter weights, and Ref. 1 is recommended if the reader is interested in pursuing the details further. When this error has been minimized, its power spectrum will be equivalent to "white" noise. Thus, the uncertainty in ϵ_n has been maximized, hence we have a maximum entropy filter.
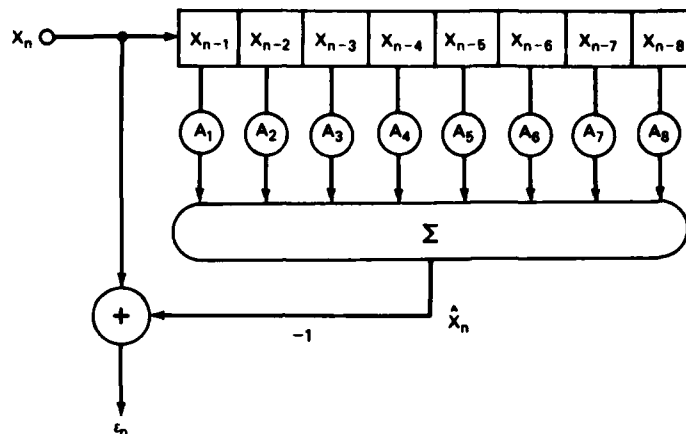
2

Fig. 1—Maximum-entropy filter with one-step linear
prediction estimator

Upon substituting Eq. (1) into Eq. (2), we readily see that we have the form of a discrete convolution

$$\epsilon_n = -\sum_{k=0}^{K} A_k X_{n-k},$$ (7)

where $A_o = -1$. The associated Z-transforms may be written,

$$\mathcal{E}(Z) = \left(1 - \sum_{k=1}^{K} A_k Z^{-k}\right) X(Z),$$ (8)

where the expression within the parentheses may be defined as the filter transform function $H(Z)$,

$$H(Z) = \left[1 - \sum_{k=1}^{K} A_k Z^{-k}\right],$$ (9)

or

$$\mathcal{E}(Z) = H(Z) \ X(Z).$$ (10)

Note that H(Z) is a polynomial in Z which will have K roots or zero factors. Since "white" noise has a power spectrum known to be equal to a constant, then from Eq. (10) it is evident that we can solve for our unknown input power spectrum if the filter function is known, i.e.,

$$| X(\omega) |^2 = \frac{| \mathcal{E}(\omega) |^2}{| H(\omega) |^2} = \frac{(\text{constant})}{\left| \prod_{k=1}^{K} (1 - D_k e^{-j\omega}) \right|^2} , \qquad (11)$$

where the peaks (poles) of the unknown power spectrum will occur at the zeros of the filter function. This permits us to model the input sequence with the powerful, discrete, all-pole, linear prediction filter illustrated in Fig. 2, both in the frequency domain and in the time domain. The prediction filter is driven by white noise.

If one considers the action of such a filter upon sinusoids corrupted with a small amount of noise, it is evident that the filter can synchronize with even a short section of the sampled time waveform of the sinusoids and, once synchronized, can then proceed to "predict" many additional samples of the waveform with little error.·

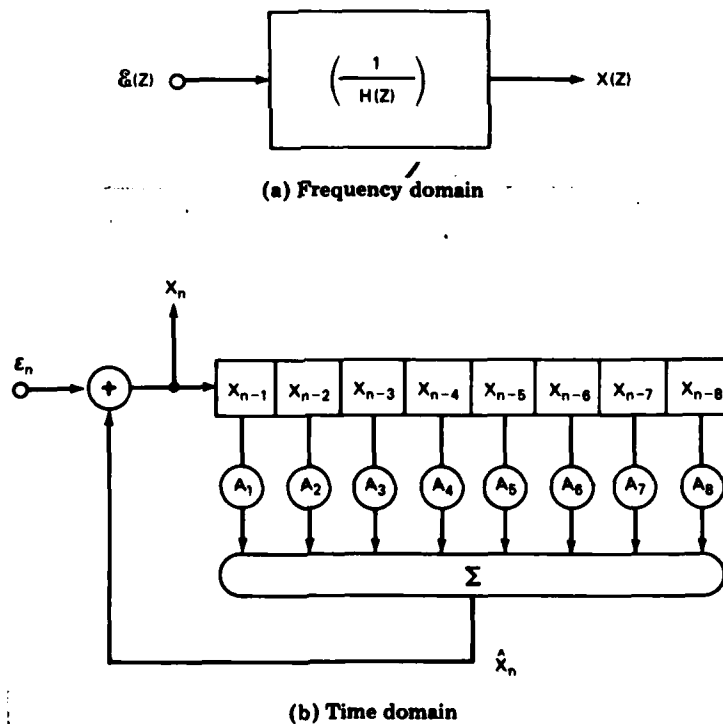
(a) Frequency domain

(b) Time domain

Fig. 2—Discrete all-pole linear prediction filter model

Another aspect of this filter is that it is a deconvolution filter, so-called because it estimates the unknown spectrum directly from the reciprocal of the filter transform function. Note in Eq. (10) that the error spectrum results from a simple multiplication of the unknown spectrum with the filter function, and that no convolution of the two occurs. In the conventional windowed Fourier transform method, on the other hand, the unknown spectrum is estimated by convolving the spectrum with the window filter transform function, and the convolution usually smears or destroys the fine detail of peaked spectra.

Reference 1 is recommended for those readers who want additional information on spectrum estimation filters.

LINEAR PREDICTION FILTERS AND ADAPTIVE SIDELOBE CANCELLERS

Conversion of the above MESA linear prediction filter to a weighted linear array of spatial sensors is straightforward, with the simplest configuration illustrated in Fig. 3. The element signal samples will be correlated in both space and time, giving rise to a two-dimensional data problem, but we convert this to spatial domain only by assuming that narrowband filtering precedes our spatial domain processing. For example, one could perform fast Fourier transform (FFT) on the element data prior to spatial processing. Also, we assume that our elements are equally spaced.

The nth "snapshot" signal sample at the kth element will consist of independent Gaussian receiver noise η_{kn} plus I incoherent source voltages,

$$E_{kn} = \eta_{kn} + \sum_{i=1}^{I} J_i \, e^{j(ku_i + \phi_{in})} \qquad 1 \leqslant k \leqslant K, \tag{12}$$

where
$$u_i = 2\pi \left(\frac{d}{\lambda}\right) \sin \theta_i$$

d = element spacing, assumed near $\lambda/2$

λ = wavelength

θ_i = spatial location angle of ith source

J_i = amplitude of ith source†

ϕ_{in} = random phase of ith source, nth sample

k = element index

n = snapshot sample index.

A "snapshot" is defined as one simultaneous sampling of the aperture signals at all array elements, and we assume that N snapshots of data are available.

---

†J_i has a constant rather than random amplitude because of a concurrent measurement program involving CW sources sampled at random times.

5

A brief examination of Fig. 3 from the standpoint of adaptive arrays leads to the conclusion that it is identical in configuration to a special subclass commonly referred to in the literature as a *sidelobe canceller* [13,14]. A typical sidelobe canceller configuration from Applebaum [14] is illustrated in Fig. 4. For the benefit of those who may not be familiar with them, it should be noted that the unweighted main-beam "element" is usually different and of much higher gain than the others, and the elements may or may not be equally spaced. They are designed to be operated on the basis of many successive snapshots (assuming digital operation) because their environment generally involves weak desired signals and an abundance of interference source data. They are a prediction filter in the sense that, after convergence, they are predicting the signal at the phase center of the main-beam element.

The adaptive sidelobe canceller is pertinent to our linear prediction filter because its spatial filter pattern analysis is well developed and can be applied directly to achieve a better understanding of the superresolution performance behavior. A further point is that real-time operation is readily achieved via most of the current adaptive algorithms, provided that the number of snapshots is enough to reach convergence in whitening ϵ. Convergence may require as few as two snapshots or as many as several thousand, depending on the particular algorithm and the parameters of the source distribution. Several examples will be discussed.

SPATIAL FILTER PATTERNS

The spatial filter function for the array of Fig. 3 is simply the adapted pattern after convergence, which is commonly referred to as the steady-state adapted pattern and may readily be computed from the inverse of the sample covariance matrix [14],

$$W_o = \mu M^{-1} S^*$$ (13)

$$S^{*t} = [0,0,0,0,0,0,0,1]$$ (14)

$$M = \frac{1}{N} \sum_{n=1}^{N} M_n$$ (15)

$$M_n = \left[E_n^* \cdot E_n^t \right],$$ (16)

where E_n is the nth "snapshot" signal sample vector whose components are given by Eq. (12), M_n is the nth snapshot contribution to the covariance matrix, M is the sample covariance matrix averaged over N snapshots, S^* is the quiescent weight steering vector, μ is a scalar quantity, and W_o is the optimum weight vector. Note that the steering vector S^* injects zero weight on every element except for the end element, causing the quiescent pattern of the array to be that of the single end element.
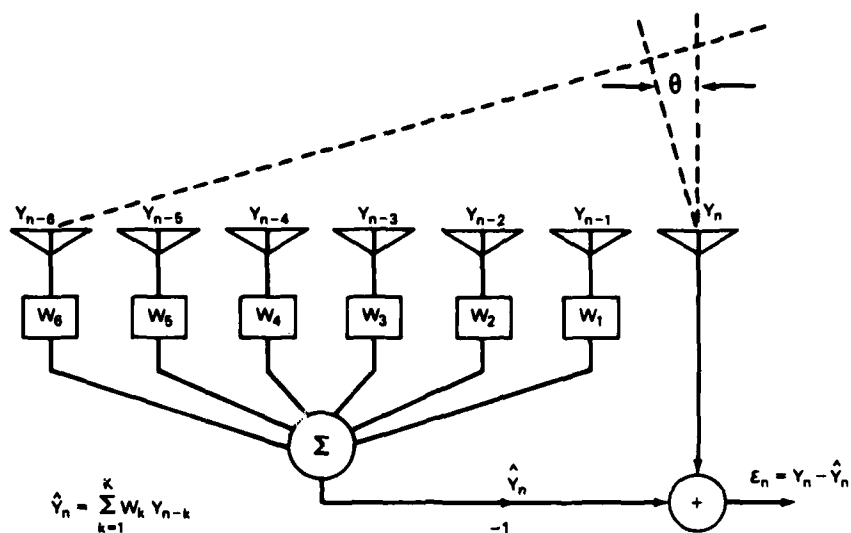
$$\hat{Y}_n = \sum_{k=1}^{\check{K}} W_k \, Y_{n-k}$$

$$\varepsilon_n = Y_n - \hat{Y}_n$$

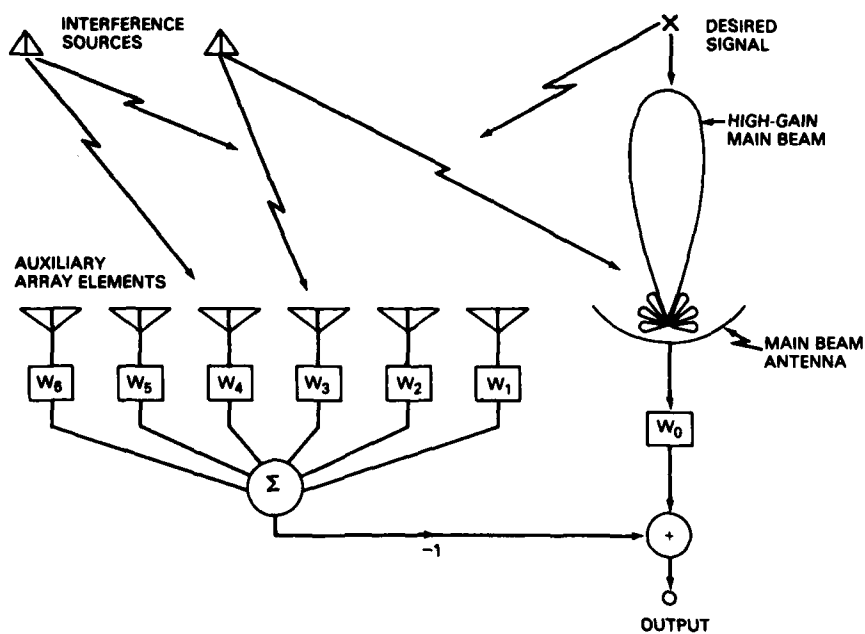Fig. 3—Array aperture linear prediction spatial filter model

Fig. 4—Typical adaptive array sidelobe canceller configuration

7

Figure 5 shows a typical quiescent (single-element) pattern and an adapted pattern obtained from an 8-element linear array with two far-field, incoherent, 30-dB sources located at 18° and 22°. The adapted pattern weights were computed per Eq. (13) from the inverse of the covariance matrix averaged over 1024 simulated snapshots. Note that the two pattern nulls (zeros) align perfectly with the locations of the two sources. Of course, the array signals in this simulation were corrupted only by receiver noise (no element errors are included), and an average over 1024 snapshots is indeed steady state. Another important point to note is that nulls in such an adapted pattern may be located arbitrarily close together in terms of beamwidth, without violating any physical principle. Yet, because the nulls have served to locate two sources within a beamwidth, one may describe this as a "superresolution" pattern.

It is readily shown that this adapted pattern is obtained by subtracting the summed array output pattern from the element (main beam) pattern and, furthermore, that the summed array pattern consists of properly weighted "eigenvector beams" [15]. In terms of the eigenvector weights, we can express the optimum weights in the form,

$$W_o = S^* - \sum_{i=1}^{K} \left(\frac{B_i - B_o}{B_i + B_o} \right) \hat{W}_{qi} e_i \tag{17}$$

$$\hat{W}_{qi} = \left(e_i^{*t} S^* \right)$$

where e_i is the ith eigenvector of the covariance matrix, B_i is the ith eigenvalue, and B_o is the smallest eigenvalue corresponding to receiver noise power. Note that only the significant eigenvectors corresponding to $B_i > B_o$ need be considered here. An adaptive array forms one such eigenvector beam for each degree of freedom consumed in nulling out the spatial source distribution. Figure 6 shows the two eigenvector beams required for this two-source example. It should be emphasized here that the true resolution and signal gain of the array are reflected in these eigenvector beams. They demonstrate the importance of having as wide an aperture as possible because the superresolution capability in the adapted pattern is a percentage of the true resolution of these beams. Also, since the superresolution nulls are formed by subtracting these beams of conventional width, it follows that the nulls will be rather delicate and very sensitive to system imperfections and signal fluctuations.

The desired "spatial spectrum pattern" is then obtained from Eq. (11) as simply the inverse of the adapted pattern. Figure 7 shows this inverse for the two-source example and compares it with the output of a conventional beam scanned through the two sources. Several comments are in order concerning such inverse patterns.

1. They are not true antenna patterns because there is no combination of the element weights that could produce such a peaked spatial pattern. They are simply a function computed from the reciprocal of a true antenna pattern.

2. Linear superposition does not hold in either the inverse or the original adapted pattern because of the nonlinear processing involved in the inverse of the covariance matrix (or the equivalent).
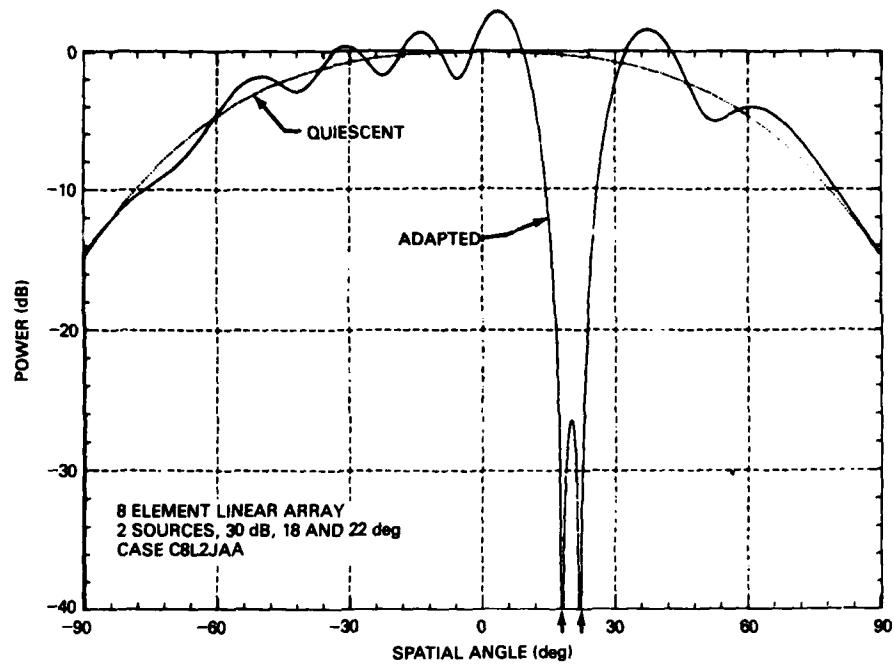
8

Fig. 5—Quiescent (single-element) and adapted patterns for two-source case, covariance
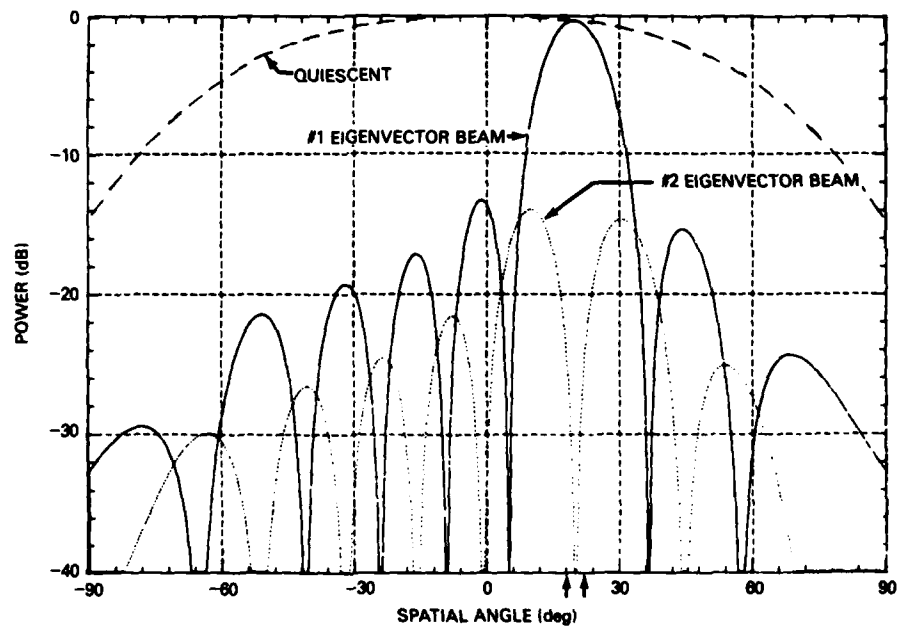matrix inverse algorithm, 1024 datasnaps

Fig. 6—Eigenvector component beam patterns for the two-source case of Fig. 5
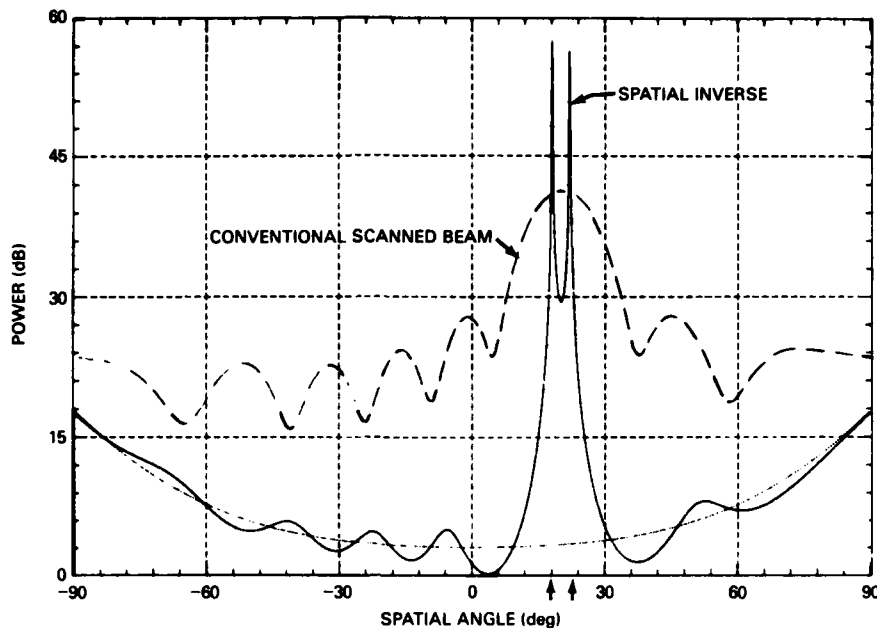
9

Fig. 7—Spatial spectrum inverse pattern for the two-source case of Fig. 5, and comparison with output of conventional scanned beam

3. The heights of the peaks do not correspond with the relative strengths of the sources because the depths of the adapted pattern nulls do not. In general, the adaptive null depth will be proportional to the square of the SNR of a source [15], but even this relationship fails when there are multiple sources closely spaced.

4. There is no real-signal output port associated with such a pattern because it is not a true antenna pattern. An output could be simulated, of course, by implementing the equivalent all-pole filter of Fig. 2 and driving it with white noise.

5. They do emphasize the locations of the zeros (nulls) of the adaptive array filter polynomial.

6. They are inherently capable of superresolution.

7. They achieve good "contrast" with the quiescent pattern background ripple because of the aforementioned proportionality to the square of source strengths.

8. Spatial information is gained beyond that obtained from a conventional array beam scanned through the sources because the array degrees of freedom are utilized in a more effective, data-adaptive manner.

REAL-TIME FILTER OPERATION

To get a feel for real-time operation performance with realistic weight update averaging, we ran simulations in which an eight-element array had its weights computed from the simple Howells—Applebaum algorithm in recursive digital form as diagrammed in Fig. 8. The associated recursive relationship for the kth weight may be written

$$(1 + \tau) \, W_k(n) = \tau W_k(n - 1) + S_k^*(n) - \left(\frac{1}{B_o}\right) E_k^*(n) \, Y(n) \tag{18}$$

where

$$Y(n) = \sum_{k=1}^{K} E_k(n) \, W_k(n - 1). \tag{19}$$

$Y(n)$ is the current array output, $E_k(n)$ is the current snapshot signal sample at the kth element (similar to Eq. (12)), $W_k(n-1)$ is the previous value of the kth weight, $S_k^*(n)$ is the injected kth beam-steering weight, and B_o is a constant equal to receiver noise power.

The digital integration loop shown in Fig. 8 is designed to simulate a simple low-pass RC filter with a time constant of τ, but we choose to make τ dynamic to get faster convergence for most situations. Thus, let τ become $\tau(n)$,
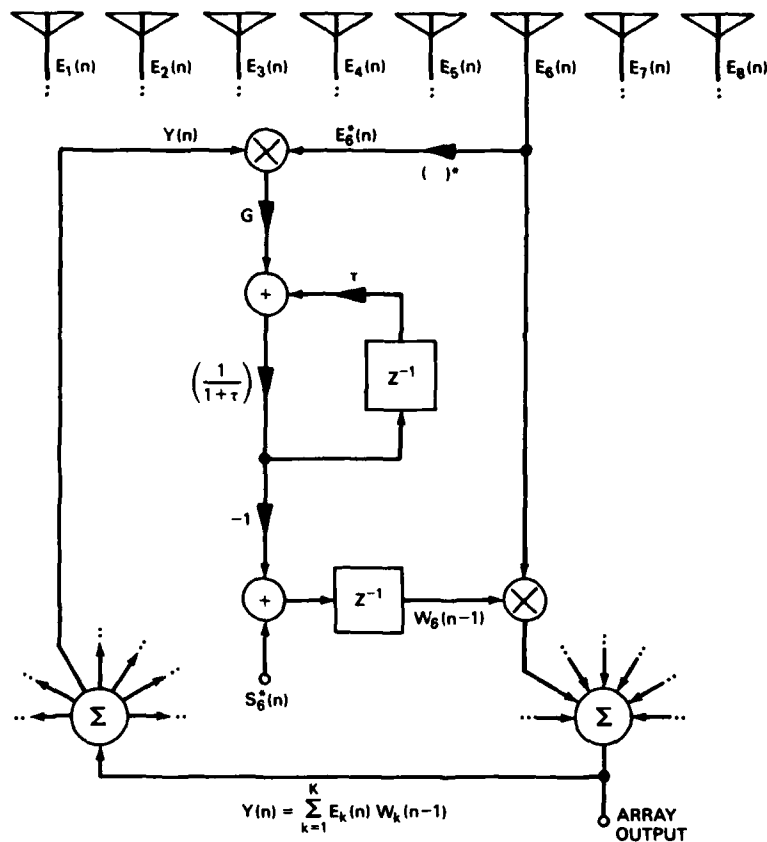
$$\tau(n) = \tau_o + TP_r(n) \tag{20}$$

where

$$T \quad = \text{high-power, fast time constant}$$

$$\tau_o \quad = \text{quiescent conditions, slow time constant}$$

$$P_r(n) \quad = \text{snapshot SNR (power ratio).}$$

This formulation permits us to satisfy the 10% bandwidth criterion at high power levels to avoid noisy weights [15] by choosing the value of $T = 3.2$, and yet the quiescent condition time constant need be no worse than $\tau_0 = 200$. The larger value for τ_0 is necessary in order to have a relatively stable quiescent pattern. Actual weight update averaging is performed in accordance with the reciprocal of the closed-loop bandwidth α,

11

Fig. 8—The Howells-Applebaum algorithm in a recursive digital form

$$\frac{1}{\alpha} = \frac{\tau}{1 + P_r(n)} = \frac{\tau_o + TP_r(n)}{1 + P_r(n)} \quad , \tag{21}$$

where we approach the value $\tau_o/2$ under quiescent conditions when $P_r = 1$, and we approach the value of T when $P_r \gg 1$.

A typical time plot of snapshot output power in decibels above receiver noise level is illustrated in Fig. 9 for the case of two 30-dB sources located at $18°$ and $22°$. Note that the system converges and nulls out the two strong sources within about 60 snapshots after processing commences. For comparison, the rms orthonormal eigenvector solution is also shown plotted, but this solution used a fixed $\tau = 48,000$ and does not converge as rapidly. The principal point demonstrated here is that convergence occurs reasonably fast in terms of snapshot counts, even for this simple LMS adaptive algorithm and, after convergence,
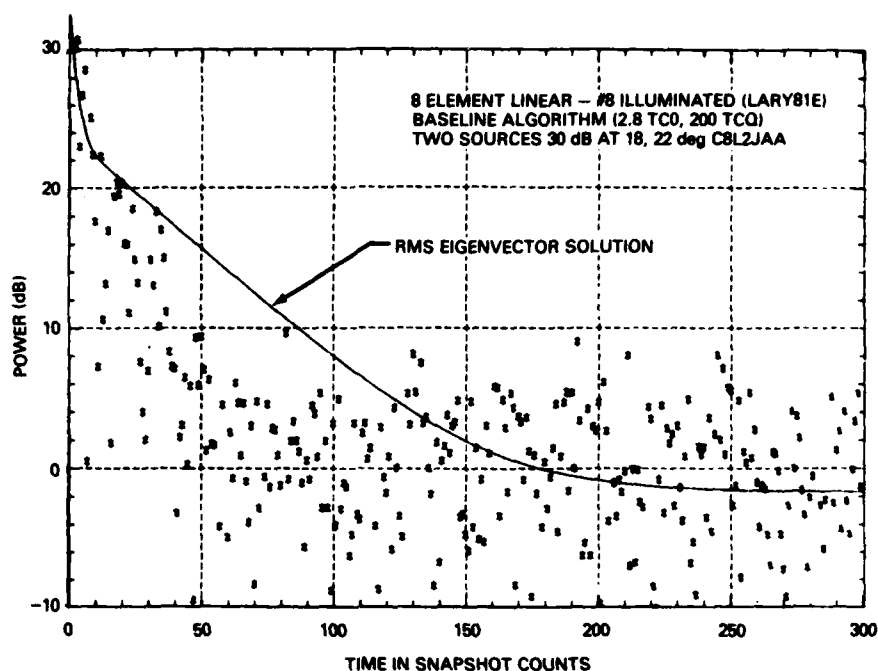
12

Fig. 9—Time-sequence snapshot output of array in decibels above receiver noise power;
Howells-Applebaum recursive algorithm with dynamic time constant

any of the snapshot weight sets can be used to compute the spatial spectrum. Figure 10
shows the spatial spectrum plots associated with snapshots 100, 200, and 300. In comparing
Fig. 10 against Fig. 7, note that the pattern has changed very little, in spite of the fact that
the integration or averaging has been reduced by two orders of magnitude, i.e., from a value
of 1024 snapshots in Fig. 7 to about 3 snapshots in Fig. 10 (albeit a decaying average in-
herent in the low-pass filter). The greatest effect of this reduced averaging is that the heights
of the peaks are reduced and the peaks fluctuate from snapshot to snapshot because of the
perturbation of the noise on each snapshot weight update.

In rounding out the example of these two incoherent sources spaced 4° apart (about
0.27 beamwidths apart), Fig. 11 illustrates what happens as we reduce the SNR strength
of the sources. Figure 11a at 20 dB shows increasing peak fluctuations in magnitude, which
merely reflect the null fluctuations in the adapted pattern, although the spatial locations
of the sources are still accurate. Figure 11b at 10 dB shows even greater fluctuations in peak
magnitude, but now the patterns are deteriorating in both shape and peak locations, indi-
cating that the resolution capability is nearing its limit, i.e., if the source power levels are
reduced further, then the adaptive array can no longer resolve them accurately at that
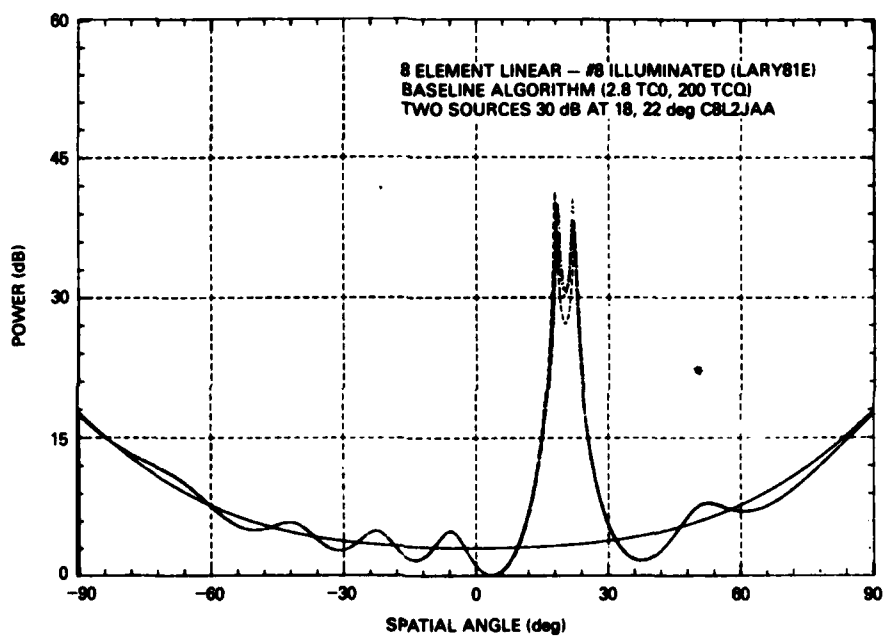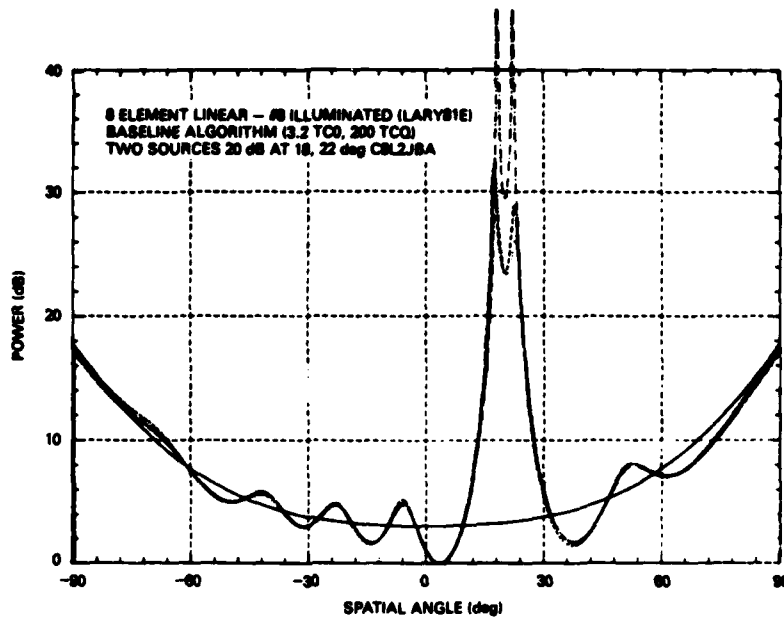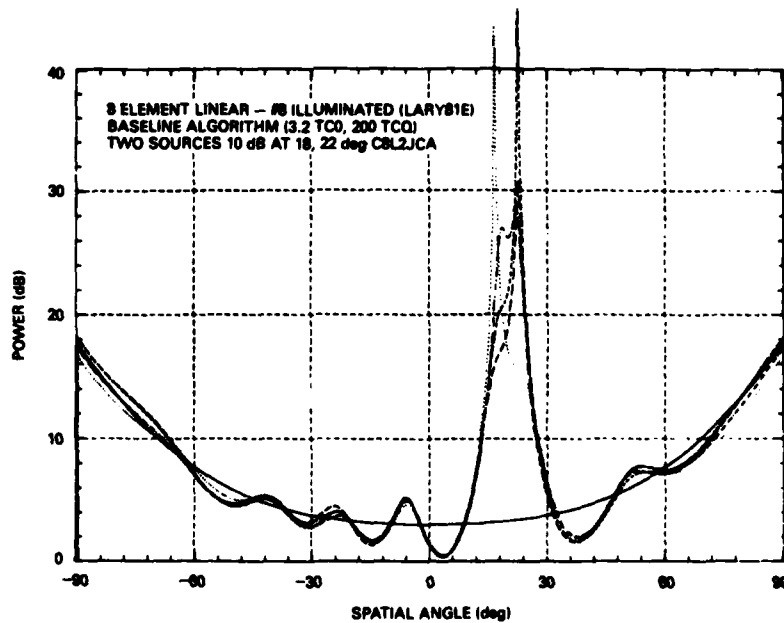particular spacing.

13

Fig. 10—Typical spatial spectrum snapshot plots after convergence, snapshot weight sets 100, 200, and 300. Two 30-dB sources were located at 18° and 22°

(a) 20-dB SNR sources

(b) 10-dB SNR sources

Fig. 11—Typical spatial spectrum snapshot plots after convergence. Two sources located at 18° and 22°

15

A summary of the approximate resolution capability limit for the adaptive array spatial filter operating against two incoherent sources is shown in Fig. 12. This performance curve is universal because the abscissa is source separation in beamwidths and the ordinate is source SNR measured at the array output, i.e., element SNR multiplied by the number of elements in the array. Thus, the curve can be utilized for any number of array elements in a linear array configuration. Note that at low ordinate SNR values, we actually have negative SNR at the elements. The curve tells us that we can separate two sources at arbitrarily small spacings, provided we have sufficient SNR and, also, provided that our element data samples are sufficiently accurate. Recall that the simulations involved here did not include any element errors.

If there are more than two sources within a beamwidth, then difficulties mount rapidly and the filter null points may not accurately represent the spatial locations of the sources. For example, the above simple LMS algorithm was tested against three sources of 30-dB strength spaced 4° apart, and it could not resolve all three even after 2048 snapshots because it never converged sufficiently (the eigenvalue spread was too great). To separate the three sources in a reasonable number of snapshots requires use of an adaptive algorithm of faster convergence [16], such as the matrix inverse of Eq. (9), wherein we use a "sliding window" averaging of the sample covariance matrix, or the Gram—Schmidt algorithm

WEIGHT UPDATE INTEGRATION PER

$$\frac{1}{\alpha} = \left(\frac{\tau_0 + TP_r}{1 + P_r}\right)$$
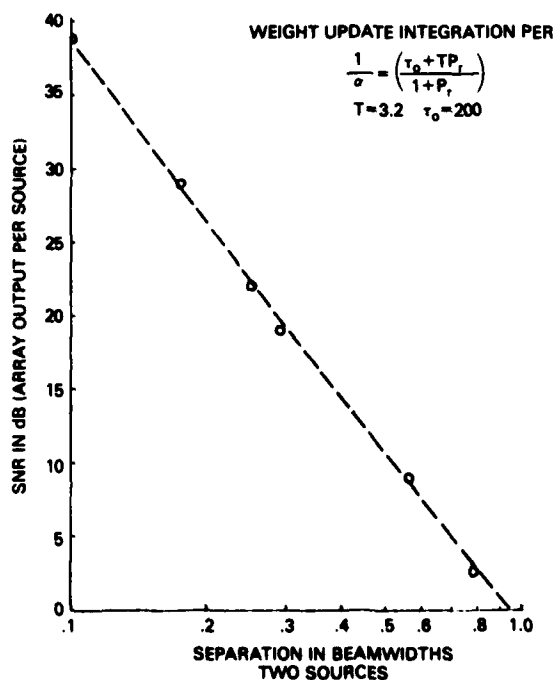
$$T = 3.2 \quad \tau_0 = 200$$

Fig. 12—Universal approximate resolution limit for two incoherent sources. Simulation conditions: narrowband, no array errors, $\lambda/2$ element spacing, linear array, Gaussian receiver noise.

16

described by Alam [11,17]. Figure 13 shows the resolution of the three sources via the Gram—Schmidt algorithm, but it should be noted that, even with this fast algorithm, resolution was not achieved until after 200 snapshots and the locations of the peaks fluctuates considerably. This was a good illustration of the "delicacy" of null formation for the case of closely spaced multiple sources.

MLM AND ADAPTIVE DIRECTIONAL CONSTRAINTS

The maximum likelihood spectral estimate is defined as a filter designed to pass the power in a narrow band about the signal frequency of interest and minimize or reject all other frequency components in an optimal manner [4,5]. This is identical to the use of a zero-order main-beam directional gain constraint in adaptive arrays [18,19], where the "spatial spectrum" would be estimated by the output residual power P_o from the optimized adapted array weights,

$$P_o = W_o^{*t} M W_o \qquad (22)$$

where

$$W_o = \mu M^{-1} S^* \text{(optimized weights)}$$

$$M = \text{covariance matrix estimate}$$

$$S^* = \text{main-beam direction-steering vector}$$

$$\mu = \text{scalar quantity.}$$

Under the zero-order gain constraint, we require $S^t W_o = 1$, whereupon μ becomes

$$\mu = (S^t M^{-1} S^*)^{-1}. \qquad (23)$$

Substituting μ and W_o into Eq. (22), then, results in

$$P_o = \frac{1}{S^t M^{-1} S^*} . \qquad (24)$$

Upon sweeping the steering vector S^* for a given covariance matrix inverse, P_o will estimate the spatial spectrum. Interestingly, this result is identical (within a constant) to the spectrum obtained from the *inverse* of the output residual power from an unconstrained optimized adapted array.

17

8 ELEMENT ARRAY — f8 ILLUMINATED (LARY81E)
GRAM-SCHMIDT ALGORITHM (32 TC0, 200 TCQ)
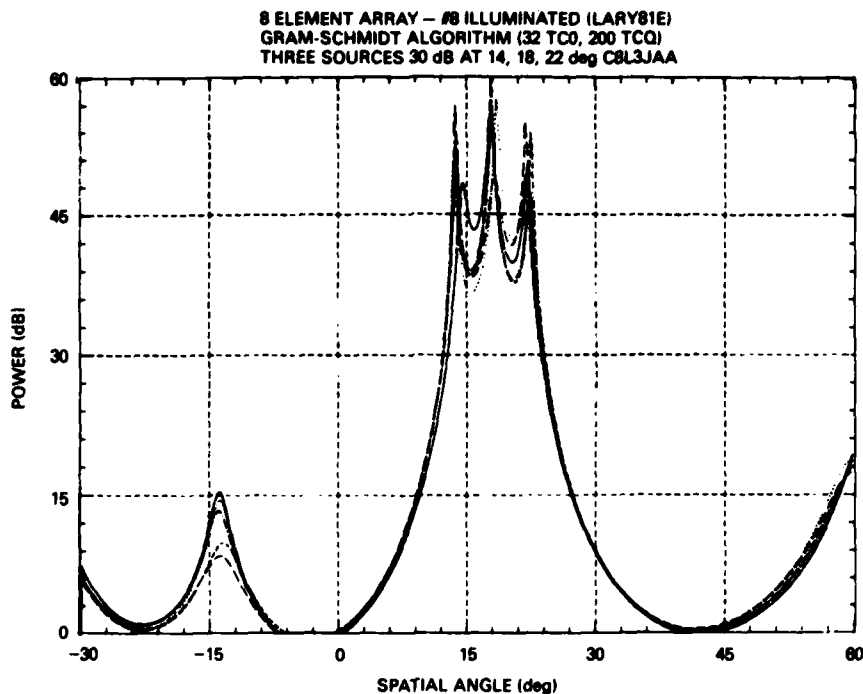THREE SOURCES 30 dB AT 14, 18, 22 deg C8L3JAA

Fig. 13—Typical spatial spectrum snapshot plots after convergence; Gram-Schmidt
algorithm, three 30-dB sources located at 14°, 18°, and 22°.

Referring back to the fourth section and the eigenvector beams shown in Fig. 6, one
may describe the principle of operation in terms of subtracting the eigenvector beams from
the quiescent uniform-illumination steering vector "main beam" for each position of the
main beam. Thus, you have a continuously changing adapted pattern as the main beam is
scanned, subject to the above gain constraint in the steering direction.

Figure 14 illustrates the output spectrum plotted from P_o for the two-source case
utilized for Figs. 5, 6, and 7. Note that in comparison with Fig. 7, this MLM spectrum has
peaks that are about 18 dB lower and are thus of lower resolution capability. However, the
two peaks have located the sources correctly and, in addition, the peak values reflect the
true power levels of the sources. This is in agreement with the observations of Lacoss [5]
and others. Although this technique has poorer resolution than the previous one and requires
more computation in plotting the output spectrum, it does offer several rather significant
advantages.

1. The output power is directly referenced to receiver noise power, thus permitting
calibration and measurement of relative source strength.

2. If the sources can be resolved, then a psuedolinear superposition holds at the peaks,
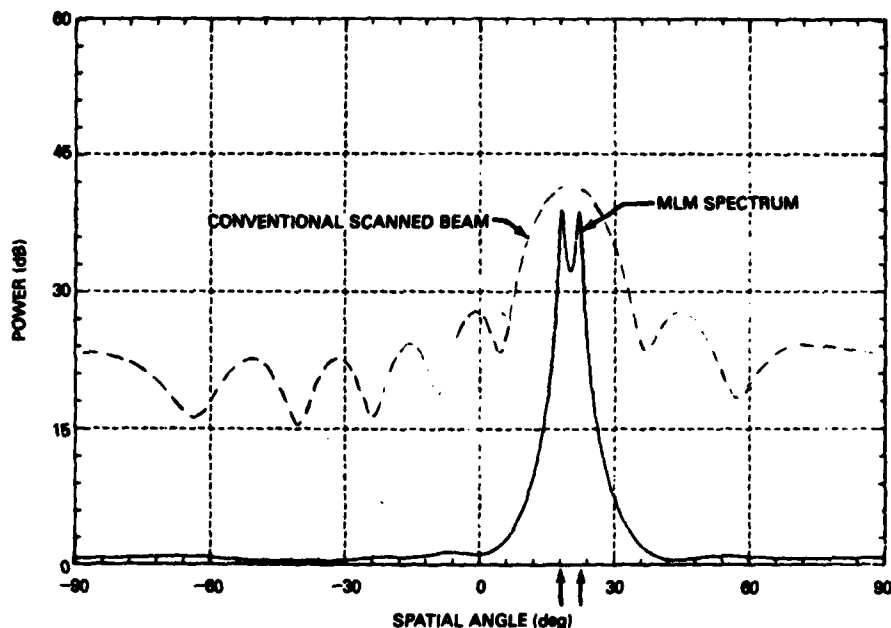and they should reflect the true relative source strengths.

18

Fig. 14—MLM spatial spectrum plotted from residual power of adaptive zero-order main-beam constraint for the two-source case of Fig. 5

3. The output of this filter is a real signal, and if the filter passband is steered to a particular source, one can monitor that source at full array gain while rejecting outputs of all other sources.

4. The residual background spatial ripple is very low and well behaved.

5. It is not necessary to have the elements equally spaced. Thus, one should take advantage of this property to spread them out for a wider aperture and substantially increase the resolution for a given number of elements. (This is done in the field of geophysics [4].) If this is done, it is very likely that this method could equal or surpass the resolution of the previous technique.

ALTERNATE ADAPTIVE PROCESSING FOR SPATIAL SPECTRA

Phase Center Prediction

The adaptive array processing described in the fourth section did not use the configuration of Fig. 3 in the true sense of a K-point linear prediction filter that runs across a larger aperture of data samples. The K elements involved were the total aperture, and a series of N snapshots of data were used to estimate or predict the signal at the phase center of the unweighted main-beam element. Phase-center prediction of this type is very flexible in that

the location of the phase center of the main beam is rather arbitrary, and it is not necessary for the elements to be equally spaced. For example, the main beam may be a weighted summation of some or all of the elements in the array.

If phase-center prediction is carried to its logical conclusion from the standpoint of estimating spatial spectra, it would appear that the ideal element configuration is a circular aperture array with an omni-mode main beam, i.e., the array would be predicting to the exact center of the circle. An example of such an array is contained in Ref. 15, and it could readily utilize the processing described in the previous two sections.

The "Thermal Noise" Algorithm

In discussing the MLM spectral estimate in the preceding section and its identical relationship to a zero-order, main-beam, directional constraint, it was mentioned that Eq. (24) was equal (within a constant) to the spectrum obtained from the inverse of the output residual power from an unconstrained optimized adapted array. If we define this output residual power as R_o, then

$$R_o = \left(S^t W_o \right) = \mu \left(S^t M^{-1} S^* \right) , \qquad (25)$$

and we have the reciprocal relationship to Eq. (24) except for μ.

An interesting feature about R_o is that it approaches zero whenever the steering vector sweeps through the position of a source, and the reason it approaches zero is that the optimum weight vector W_o approaches zero. Therefore, it appears prudent to formulate the dot product of W_o with its own conjugate and define this product as the adapted thermal noise power output N_o,

$$N_o = W_o^{*t} W_o. \qquad (26)$$

The reciprocal of N_o then estimates the spatial spectrum, and we may refer to this as the "thermal noise" algorithm for spectrum estimation. Figure 15 illustrates the application of this algorithm to the same two-source case as was used for Figs. 5, 6, 7, and 14. Contrasting it with the equivalent MESA and MLM techniques, note that it exhibits resolution peaks fully equal to MESA, and yet retains the very low residual background ripple of MLM referenced to quiescent receiver noise power level. Like MESA, it cannot measure relative source strength, but it should be proportional to the square of source strengths whenever it can resolve the sources. Thus, the "thermal noise" algorithm appears to possess an interesting combination of the characteristics of both MESA and MLM.
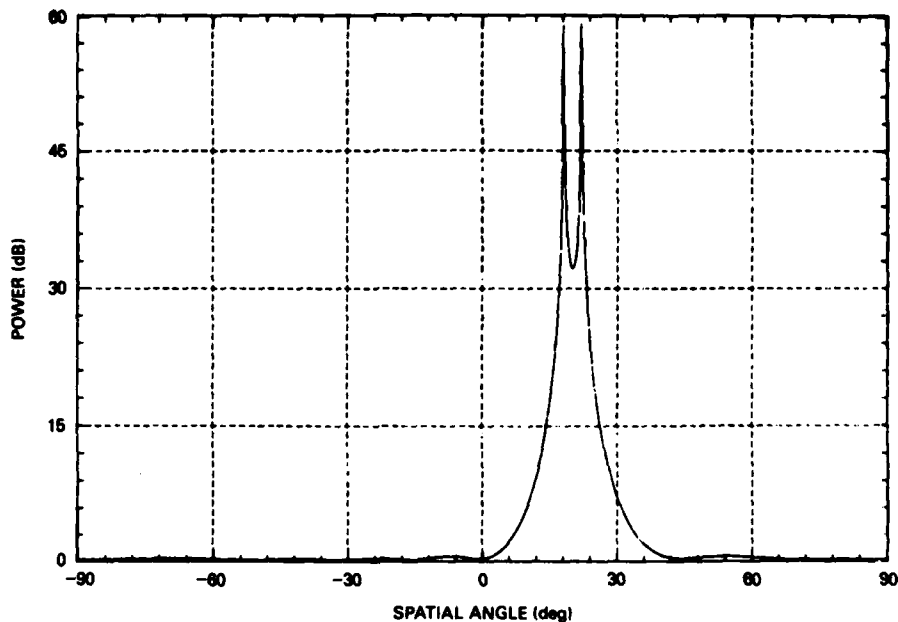
Fig. 15—"Thermal noise" algorithm spatial spectrum plotted for the two-source case of Fig. 5

SIGNIFICANT PROCESSING DIFFERENCES

Although the similarities are extensive enough to create a favorable climate for technique interchanges, there are also some significant differences which arise from the very nature of the applications and their data. For example, assume that we utilize the Burg MESA technique to run a K-point prediction filter across an RF aperture of M elements, where K must be smaller than M by at least 50% in order to obtain a reasonable averaged estimate for determination of the K filter weights. This type of processing has a great advantage in being able to operate with a single snapshot of element data, but it is "unthinkable" from an RF array point of view because it is wasting expensive aperture elements. It is far more preferable to operate on the basis of many snapshots of data from the smallest number of elements possible. In fact, a recent study of the Burg MESA technique by King [8], as applied to an RF spatial array, found that single snapshot results were seldom satisfactory, and that it was usually necessary to average the results from 10 or 20 snapshots in order to achieve a stable spectrum estimate. This comment is not meant to imply that the Burg technique is not applicable, but only that single-snapshot operation is not very practical for RF arrays.

A related difference is simply the fact that RF array element signal samples are correlated in both space and time, thus giving rise to a two-dimensional data problem [7] that does not exist in spectrum analysis. To overcome this problem usually requires filtering in both domains. For example, one may handle the time domain via tapped delay lines, an FFT operation, or actual narrowband filters at each array element. Note that, in each case,

21

we imply many aperture snapshots in order to handle this two-dimensional data problem. Fortunately, the applications of RF array systems are such as to produce an abundance of data snapshots, so that processing is naturally designed to operate on this premise.

Another area of significant difference is the manner in which correlation matrix coefficients are estimated. In spectral analysis, one generally deals with a single data sequence in X_n of M samples, from which is computed the autocorrelation matrix coefficients of the form

$$\phi_\tau = \frac{1}{M} \sum_{n=0}^{N-\tau-1} X_n X_{n+\tau}^*, \qquad 0 \leqslant \tau \leqslant L \qquad (27)$$

where the lag τ is restricted to some maximum value L, which is a fraction of M. In adaptive array processing, on the other hand, one generally deals with N snapshots of data sampled from K elements, from which is computed covariance matrix coefficients of the form

$$\phi_{kl} = \frac{1}{N} \sum_{n=1}^{N} X_{kn}^* X_{ln} \qquad \begin{array}{l} 1 \leqslant k \leqslant K \\ 1 \leqslant l \leqslant K. \end{array} \qquad (28)$$

Equations (27) and (28) represent two different types of interelement signal correlation averages, and they can lead to different spectrum estimates, particularly if coherence exists among the spatial sources.

Therefore, some care must be exercised when borrowing a given technique from one field for use in the other.

CONCLUSIONS

The Burg MESA and MLM nonlinear spectral analysis techniques have been related to their similar nonlinear adaptive array antenna counterparts, which consist of the sidelobe canceller and directional gain constraint techniques. The comparison study was conducted in the interest of achieving some cross-fertilization by examining their principles of operation from the antenna array spatial pattern viewpoint, and the analysis helps to qualify their superresolution performance behavior. It was shown that the superresolution derives from the subtraction of eigenvector beams that embody the true conventional resolution and signal gain of the array, such that physical principles are not really violated. Resolution is still proportional to the width of the array aperture. The spatial spectrum patterns are not true antenna patterns but are simply the inverse of the adaptive filter patterns. They are capable of superresolution, and spatial information is gained beyond that obtained from a conventional array beam, which is scanned through the sources.

The adaptive array counterpart is naturally suited to real-time spectral estimation via most of the current adaptive algorithms, and the case of two incoherent sources located within a beamwidth was simulated over a SNR range of 0 to 40 dB. A universal super-resolution performance curve, Fig. 12, was developed for this particular case, which can be utilized for linear arrays of any number of elements. If there are more than two sources within a beamwidth, difficulties mount rapidly and the filter null points may not accurately represent source locations.

In addition to the direct adaptive counterparts, two alternate adaptive spatial spectrum estimators were suggested. One is a circular array aperture arrangement which predicts to the center of the circle, and the other is a new adaptive "thermal noise" algorithm which appears to possess an interesting combination of both MESA and MLM characteristics.

There are some significant differences between spectral analysis techniques and adaptive array techniques that relate to the nature of their applications and the two-dimensional data problem. However, it appears that there is much to be gained through careful analysis of the other's techniques. For example, in addition to the obvious applications in target detection, DF (direction finding) systems, and source classification, spectral analysis techniques should be of benefit in data extension and coherence effects investigations.

REFERENCES

1. *Modern Spectrum Analysis*, D. G. Childers, ed., IEEE Press, New York, 1978. (Note: This book contains complete copies of references 2–7, 9, 11, 12.)

2. J. P. Burg, "Maximum Entropy Spectral Analysis," in *Proc. 37th Meeting of the Society of Exploration Geophysicists*, 1967, Oklahoma City.

3. J. P. Burg, "A New Analysis Technique for Time Series Data," Paper presented at the NATO Advanced Study Institute on Signal Processing with Emphasis on Underwater Acoustics, Enschede, Netherlands, 1968.

4. J. Capon, "High-Resolution Frequency-Wavenumber Spectrum Analysis," *Proc. IEEE* 57, 1408–1418 (Aug. 1969).

5. R. T. Lacoss, "Data Adaptive Spectral Analysis Methods," *Geophysics* 36, 661–675 (Aug. 1971).

6. J. P. Burg, "The Relationship between Maximum Entropy Spectra and Maximum Likelihood Spectra," *Geophysics* 37, 375–376 (Apr. 1972).

7. R. N. McDonough, "Maximum-Entropy Spatial Processing of Array Data," *Geophysics* 39, 843–851 (Dec. 1974).

8. W. R. King, "Maximum Entropy Wavenumber Analysis," NRL Report 8298, Mar. 1979.

9. L. J. Griffiths, "Rapid Measurement of Digital Instantaneous Frequency," *IEEE Trans.* ASSP-23, 207—222 (Apr. 1975).

10. D. R. Morgan and S. E. Craig, "Real-Time Adaptive Linear Prediction Using the Least Mean Square Gradient Algorithm," *IEEE Trans.* ASSP-24, 494—507 (Dec. 1976).

11. M. A. Alam, "Adaptive Spectral Estimation," in *Proc. 1977 Joint Automatic Control Conf.*, June 1977, San Francisco, Calif.

12. A. van den Bos, "Alternative Interpretation of Maximum Entropy Spectral Analysis," *IEEE Trans.* IT-17, 493—494 (July 1971).

13. P. W. Howells, "Explorations in Fixed and Adaptive Resolution at GE and SURC," *IEEE Trans.* AP-24, 575—584 (Sept. 1976).

14. S. P. Applebaum, "Adaptive Arrays," *IEEE Trans.* AP-24, 585—598 (Sept. 1976).

15. W. F. Gabriel, "Adaptive Arrays—An Introduction," *Proc. IEEE* 64, 239—272 (Feb. 1976).

16. I. S. Reed, J. D. Mallett, and L. E. Brennan, "Rapid Convergence Rate in Adaptive Arrays," *IEEE Trans.* AES-10, 853—863 (Nov. 1974).

17. M. A. Alam, "Orthonormal Lattice Filter—A Multistage Multichannel Estimation Technique," *Geophysics* 43, 1368—1383 (Dec. 1978).

18. O. L. Frost, III, "An Algorithm for Linearly Constrained Adaptive Array Processing," *Proc. IEEE.* 60, 926—935 (Aug. 1972).

19. S. P. Applebaum and D. J. Chapman, "Adaptive Arrays with Main Beam Constraints," *IEEE Trans.* AP-24, 650—662 (Sept. 1976).